



# A general, accurate procedure for calculating molecular interaction force

Pinghai Yang, Xiaoping Qian \*

Department of Mechanical, Materials and Aerospace Engineering, Illinois Institute of Technology, Chicago, IL 60616, USA

## ARTICLE INFO

### Article history:

Received 2 March 2009

Accepted 11 May 2009

Available online 27 May 2009

### Keywords:

van der Waals forces/energies

NURBS surface

Surface formulation

## ABSTRACT

The determination of molecular interaction forces, e.g., van der Waals force, between macroscopic bodies is of fundamental importance for understanding sintering, adhesion and fracture processes. In this paper, we develop an accurate, general procedure for van der Waals force calculation.

This approach extends a surface formulation that converts a six-dimensional (6D) volume integral into a 4D surface integral for the force calculation. It uses non-uniform rational B-spline (NURBS) surfaces to represent object surfaces. Surface integrals are then done on the parametric domain of the NURBS surfaces. It has combined advantages of NURBS surface representation and surface formulation, including (1) molecular interactions between arbitrary-shaped objects can be represented and evaluated by the NURBS model further common geometries such as spheres, cones, planes can be represented exactly and interaction forces are thus calculated accurately; (2) calculation efficiency is improved by converting the volume integral to the surface integral.

This approach is implemented and validated via its comparison with analytical solutions for simple geometries. Calculation of van der Waals force between complex geometries with surface roughness is also demonstrated. A tutorial on the NURBS approach is given in [Appendix A](#).

© 2009 Elsevier Inc. All rights reserved.

## 1. Introduction

The determination of molecular interaction forces, e.g., van der Waals force, between macroscopic bodies is of fundamental importance to many scientific fields, e.g., surface, interface and colloidal sciences for understanding sintering, adhesion and fracture processes, and for diverse applications such as precise manipulation of micro/nano objects in nanotechnology, resolving stiction in MEMS and semiconductor industry, and in pharmaceutical manufacturing. This paper focuses on the calculation of van der Waals interactions.

The van der Waals forces calculation has been investigated extensively since early last century. However, the analysis and discussion of modeling and simulation of the van der Waals force are thus far limited to objects with simple geometries or those that can be simplified to simple geometries under some assumptions. For example, analytical formulae for computing molecular interactions exist between sphere–sphere [5], sphere–half space [4,6,7] and cone–half space [2]. Numerical simulation based on a double volume integral has been conducted for interactions between sphere–block [6] and sphere–needle tip [9]. However, all these analytical and numerical solutions are valid only for their specific and simple geometries. The fundamental challenge in extending these solutions to more general geometries is due to the six-dimensional (6D), double volume integral (Eq. (3)), which is very difficult to compute either analytically or numerically. Analytically,

the 6D double volume integral makes it difficult to evaluate van der Waals forces beyond simple geometries. Numerically, the double volume integral makes its difficult to track the solution accuracy and the computing efficiency.

Consequently, these shape-specific solutions are thus far restricted to simple geometric shapes and not applicable to general object geometry. It severely restricts the applicability of these methods since real nanoscale objects may not be of simple geometry and they contain surface roughness. Previous researches have shown that even a relatively small surface roughness would have a large impact on the van der Waals force [12,14]. Therefore a method that can calculate the van der Waals force accurately and is applicable to general shape is desirable for many applications.

In this paper, we present a procedure for calculating van der Waals force that is both accurate and applicable to general shapes including both common geometries and freeform shapes. Our approach extends a recent surface formulation approach [3] that converts a 6D volume integral into a 4D surface integral for the force calculation. Our approach uses non-uniform rational B-spline (NURBS) surfaces to represent object surfaces. Surface integrals are then done on the parametric domain of the NURBS surfaces. When compared with existing approaches, our calculation procedure has the following advantages:

- *Applicable to general shapes.* NURBS surface representation, the standard surface representation used in computer-aided design (CAD) systems, can represent common geometries such as spheres in nano-particles, cylinders in nano-rods, disk-swept

\* Corresponding author.

E-mail address: [qian@iit.edu](mailto:qian@iit.edu) (X. Qian).

**Nomenclature**

<b>A</b>	Hamaker constant	<b>F/F</b>	van der Waals force between two bodies
<b>C</b>	London–van der Waals constant	<b>s</b>	distance between the two atoms/molecules
$\rho_i$	atomic density of body <i>i</i>	<b>S</b>	NURBS surface
$w_{vdw}$	energy potential between two atoms/molecules	$\mathbf{p}_{i,j}$	control points of NURBS surfaces
<b>E</b>	van der Waals energy between an atom/molecule and a body	$w_{i,j}$	weights of NURBS surfaces
<b>f</b>	van der Waals force between two atoms/molecules	<b>U,V</b>	knot vectors of NURBS surfaces
		<b>n</b>	surface normal

shape in nano-wires, and other shapes such as cone, torus, ellipsoid, and plane exactly. It can also conveniently represent free-form geometry e.g., objects with surface roughness.

- *High accuracy.* Since molecular interactions fall off rapidly (at a rate of inverse power of six) over the separation distance, any small discrepancy between Gaussian quadrature points used in the surface integration and the underlying surface would lead to a significant bias in the resulting force. NURBS surfaces can represent common geometry exactly and the Gaussian quadrature points used in our surface integration lie exactly on the surface, i.e., without any geometric approximation error. NURBS surfaces can also be subdivided to produce more Gaussian quadrature points lying exactly on the surface to further improve the accuracy of the numerical integration. Our approach thus leads to far better accuracy than those based on the approximated geometry e.g., in mesh based approach [13].
- *Computing efficiency.* Due to the use of 4D surface integration instead of 6D volume integration, the calculation efficiency has been improved.

Fig. 1 compares the proposed NURBS surface based approach with the analytical solution to van der Waals force calculation where the first and second numerical simulations refer to the calculation for the patches before and after the subdivisions. It shows NURBS surface based approach, with patch refinement, produces accurate results. For details of this sphere–sphere interaction force calculation, please refer to Section 5.1.2.

The remainder of the paper is organized as follows. Section 2 briefly introduces the van der Waals force calculation. In Section 3, we introduce the NURBS surface as our underlying representation of 3D object surfaces and discuss its salient features, which are beneficial for the van der Waals force calculation. In Section 4, we explain our van der Waals force calculation approach in details, which is based on the NURBS surface formulation. In Section 5, we present experimental examples to illustrate the accuracy and general applicability of this approach. In Section 6, we discuss its comparison with the triangular mesh based approach and the use of adaptive NURBS surface subdivision, and its error estimation and convergence analysis. We conclude this paper in Section 7.

**2. van der Waals force computing**

van der Waals force is an intermolecular force that arises from a fluctuating electromagnetic field resulting in instantaneous (electrical and magnetic) polarizations between atoms/molecules. van der Waals force has been studied extensively [8,10]. Here, we briefly present some basic concepts and formulas, upon which we have developed the NURBS surface based approach for van der Waals force computing.

The London equation is the first basic equation used to calculate the energy potential,  $w_{vdw}$ , between two atoms/molecules:

$$w_{vdw}(s) = -\frac{C}{s^6} \tag{1}$$

where *s* is the distance between the two atoms/molecules and *C* is the London–van der Waals constant, a material-dependant interaction constant between the two atoms/molecules. To account for the retardation effect, a corrected London equation is introduced [1]:

$$w_{vdw}(s) = -\frac{C}{s^6(s+c)}$$

where *c* is a constant value proportional to the “characteristic wavelength” of the interaction.

In order to validate our numerical simulation result with existing analytical solutions, we focus on calculation based on the original London equation, i.e., Eq. (1), for computing atoms/molecules energy potential since currently analytical solutions only exist for the original London equation. However, our NURBS surface based approach is applicable to both equations since both can be directly numerically evaluated with the Gaussian quadrature method.

Based on Eq. (1), the van der Waals force **f** between the two atoms/molecules is then given by:

$$\mathbf{f} = -\nabla w_{vdw} \tag{2}$$

Assuming that the two bodies have the properties of additivity, uniform material properties and continuous medium, the force between two bodies of arbitrary geometry is:

$$\mathbf{F} = \rho_1 \rho_2 \int_{V_2} \int_{V_1} \mathbf{f}(s) dV_1 dV_2, \tag{3}$$

where  $\rho_i$ , *i* = 1, 2 is the atomic density of body *i*. Eq. (3) can be rewritten as:

$$\mathbf{F} = -C \cdot \rho_1 \rho_2 \int_{V_2} \int_{V_1} \nabla w_{vdw} dV_1 dV_2 = C \cdot \rho_1 \rho_2 \int_{V_2} \int_{V_1} \nabla \frac{1}{s^6} dV_1 dV_2 \tag{4}$$

Similarly, the energy of van der Waals interaction between an atom/molecule and an arbitrarily shaped body is given by

$$E = C \cdot \rho_1 \int_{V_1} w_{vdw} dV_1 = -C \cdot \rho_1 \int_{V_1} \frac{1}{s^6} dV_1 \tag{5}$$

In Eq. (4), a double volume integral is involved, which is very difficult to execute either analytically or numerically.

In this paper, to reduce the computational complexity, we extend the surface formulation [3] to objects described by NURBS surfaces. This surface formulation reduces the 6D integral to 4D integral. The NURBS surface also eliminates the geometric approximation used in other surface formulation based schemes [13]. In the next two sections, we briefly introduce NURBS surfaces and then present our NURBS surface based van der Waals force computing approach.

**3. NURBS surface representation for 3D objects**

In this paper, NURBS representation is used to represent geometries of nanoscale objects and compute the van der Waals forces/energies. We give a brief overview of NURBS surface and details are commonly available in computer-aided design (CAD) and computer graphics literature such as [11].

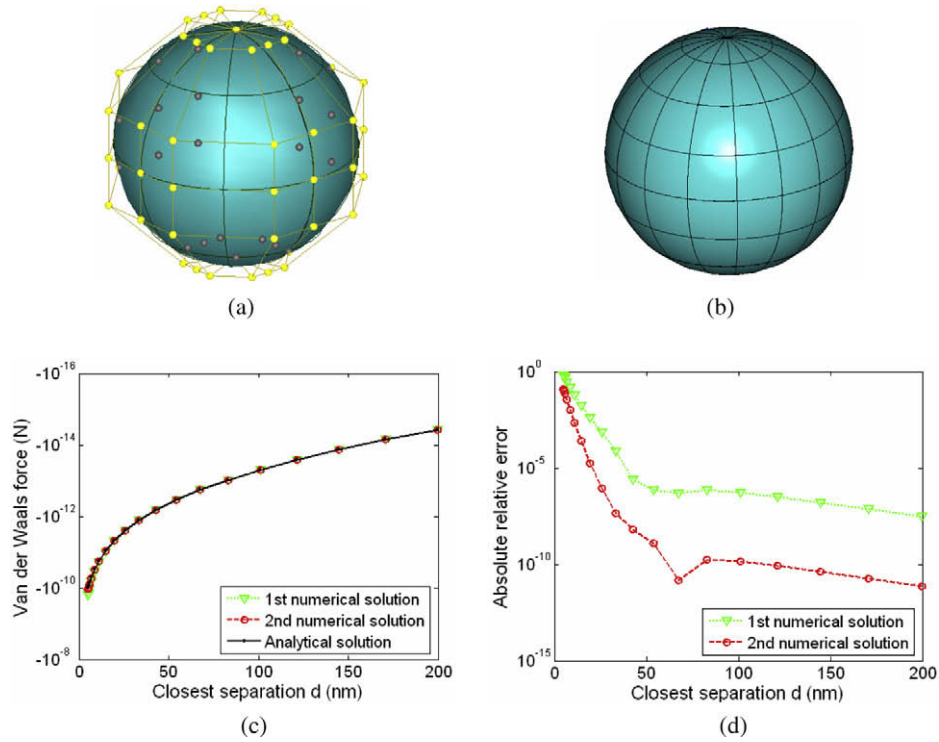


**Fig. 1.** NURBS representation based surface formulation for van der Waals force calculation: (a) NURBS representation of a sphere; (b) subdivided NURBS patches; (c) comparison of analytical solution with the numerical results; (d) relative error.

By means of tensor products, a NURBS surface can be constructed from a bidirectional net of  $(n + 1) \times (m + 1)$  control points and knot vectors  $\{u_i\}$  and  $\{v_j\}$ :

$$\mathbf{S}(u, v) = \frac{\sum_{i=0}^n \sum_{j=0}^m N_{i,p}(u) N_{j,q}(v) w_{i,j} \mathbf{p}_{i,j}}{\sum_{i=0}^n \sum_{j=0}^m N_{i,p}(u) N_{j,q}(v) w_{i,j}} \quad (6)$$

Then we can obtain a bi-variate surface over the two independent parameters  $u$  and  $v$ , where  $\mathbf{p}_{i,j}$  represent control points of the NURBS surface,  $w_{i,j}$  are the weights and  $N_{i,p}(u)$  and  $N_{j,q}(v)$  are the  $p$ th degree and  $q$ th degree B-spline basis functions defined in  $u$  and  $v$  directions, respectively. Basis function  $N_{i,p}(u)$  is defined as:

$$N_{i,0}(u) = \begin{cases} 1 & \text{if } u_i \leq u \leq u_{i+1} \\ 0 & \text{otherwise} \end{cases} \quad (7)$$

$$N_{i,p}(u) = \frac{u - u_i}{u_{i+p} - u_i} N_{i,p-1}(u) + \frac{u_{i+p+1} - u}{u_{i+p+1} - u_{i+1}} N_{i+1,p-1}(u) \quad (8)$$

where  $\mathbf{U} = \{u_0, u_1, \dots, u_{n+p+1}\}$  is the knot vector in  $u$  direction. Similarly, basis function  $N_{j,q}(v)$  is defined as:

$$N_{j,0}(v) = \begin{cases} 1 & \text{if } v_j \leq v \leq v_{j+1} \\ 0 & \text{otherwise} \end{cases} \quad (9)$$

$$N_{j,q}(v) = \frac{v - v_j}{v_{j+p} - v_j} N_{j,q-1}(v) + \frac{v_{j+q+1} - v}{v_{j+q+1} - v_{j+1}} N_{j+1,q-1}(v) \quad (10)$$

where  $\mathbf{V} = \{v_0, v_1, \dots, v_{m+q+1}\}$  is the knot vector in  $v$  direction.

Two NURBS surfaces, one spherical particle and the other a free-form surface, are illustrated in Fig. 2. The black curves on the surface are the knot curves and the yellow dots and lines represent the control points and the control polygon.

NURBS surface representation has many desirable properties [11]. We highlight below some of them that are relevant to this work.

**Property 1.** It offers one common mathematical expression for both common shapes (e.g., plane, sphere, cylinder and cone) and freeform shapes.

For example, a unit sphere, with a center located at the origin, is represented by a bi-quadratic NURBS surface as shown in Fig. 2a. Table 1 gives all the necessary parameters to create this NURBS

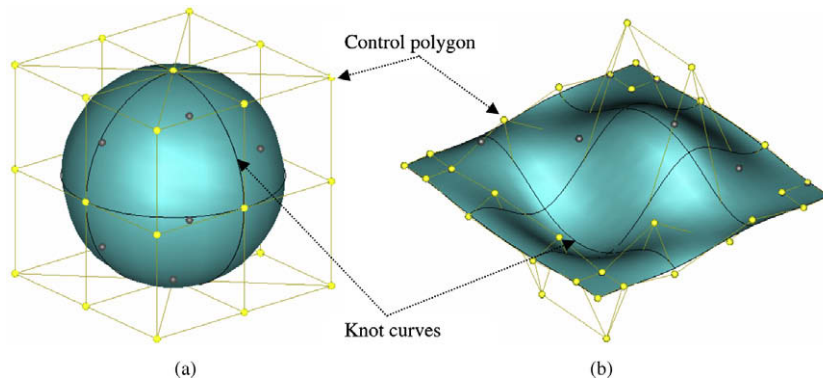


**Fig. 2.** Examples for NURBS surfaces. (a) A unit sphere; (b) a smooth freeform surface.

**Table 1**  
NURBS surface parameters for the unit sphere.

Surface type	Degree		Knot vector		Control points $\mathbf{p}_{i,j}$	Weights $w_{i,j}$
	$u$	$v$	$u$	$v$		
Sphere	2	2	{0, 0, 0, 0.25, 0.25, 0.5, 0.5, 0.75, 0.75, 1, 1, 1}	{0, 0, 0, 0.5, 0.5, 1, 1, 1}	$\mathbf{p}_{0,j} = \mathbf{p}_{8,j} = (1, 0, j - 2)$ $\mathbf{p}_{1,0} = (0, 0, -1), \mathbf{p}_{1,3} = (0, 0, 1)$ $\mathbf{p}_{1,j} = (1, 1, j - 2), \mathbf{p}_{2,j} = (0, 1, j - 2)$ $\mathbf{p}_{3,j} = (-1, 1, j - 2), \mathbf{p}_{4,j} = (-1, 0, j - 2)$ $\mathbf{p}_{5,j} = (-1, -1, j - 2), \mathbf{p}_{6,j} = (0, -1, j - 2)$ $\mathbf{p}_{7,j} = (1, -1, j - 2), i = 0 \dots 8, j = 1, 2, 3$	$w_{i,j} = 1, i = 0, 2, 4, 6, 8, j = 0, 2, 4$ $w_{i,j} = \frac{\sqrt{2}}{2}, i = 0, 2, 4, 6, 8, j = 1, 3$ $w_{i,j} = \frac{\sqrt{2}}{2}, i = 2, 4, 6, 8, j = 1, 3, 5$ $w_{i,j} = \frac{1}{2}, i = 2, 4, 6, 8, j = 2, 4$

sphere, i.e., degrees in  $u/v$  direction, 12/8 knots in  $u/v$  direction and  $9 \times 5$  control points and weights. All the NURBS spheres used in this paper can be generated based on the data in Table 1 and the NURBS surface subdivision technique.

**Property 2.** It is enclosed within the convex hull of its control polygon.

By applying this property, we can obtain the distance bound between two NURBS surfaces, which can be useful for identifying the error bound in van der Waals force/energy calculation and may enable the development of an adaptive surface subdivision scheme as discussed in Section 6.2.

**Property 3.** It is a piecewise surface composed of surface patches defined on each knot span.

This means that an NURBS surface can be divided into several NURBS patches, which are defined as NURBS surfaces without inner knots. And the NURBS patch is the basic unit for van der Waals force/energy calculation in this paper. For example, the NURBS surface shown in Fig. 2b can be divided into  $3 \times 3$  NURBS patches by the four black, inner knot curves.

#### 4. NURBS based surface formulation for van der Waals force calculation

In Eq. (2), the interaction force between two atoms/molecules is defined as the gradient of the interaction potential in terms of the distance  $s$ . Now, we further define a vector field  $\mathbf{G}$  based on the potential field

$$\nabla \cdot \mathbf{G} = -w_{vdw} \tag{11}$$

Substitution of Eqs. (2) and (11) into Eq. (3) gives a new formula for the van der Waals force between two arbitrary-shaped bodies:

$$\mathbf{F} = \rho_1 \rho_2 \int_{V_2} \int_{V_1} \nabla(\nabla \cdot \mathbf{G}) dV_1 dV_2. \tag{12}$$

Applying the divergence theorem, we obtain

$$\mathbf{F} = \rho_1 \rho_2 \int_{S_2} \int_{S_1} (\mathbf{G} \cdot \mathbf{n}_1) \cdot \mathbf{n}_2 dS_1 dS_2 \tag{13}$$

where  $\mathbf{n}_1$  and  $\mathbf{n}_2$  represent the outward unit normal field of the nano-bodies 1 and 2,  $S_1$  and  $S_2$  represent the boundary surfaces of the nano-bodies 1 and 2, which are NURBS surfaces oriented by outward-pointing normals.

From NURBS surface Property 3, we easily see that these two NURBS surfaces  $S_1$  and  $S_2$  are piecewise surfaces with  $(n_1 - p_1) \times (m_1 - q_1)$  and  $(n_2 - p_2) \times (m_2 - q_2)$  component NURBS patches, respectively, where  $n_i$  and  $m_i$  represent the number of control points in  $u$  and  $v$  direction,  $p_i$  and  $q_i$  represent the degree of the basis functions in  $u$  and  $v$  direction. Hence, Eq. (13) can be rewritten as:

$$\mathbf{F} = \rho_1 \rho_2 \sum_{i_1=1}^{n_1-p_1} \sum_{j_1=1}^{m_1-q_1} \sum_{i_2=1}^{n_2-p_2} \sum_{j_2=1}^{m_2-q_2} \int_{S_{2j_2}} \int_{S_{1j_1}} (\mathbf{G} \cdot \mathbf{n}_{i_1 j_1}) \cdot \mathbf{n}_{i_2 j_2} dS_{i_1 j_1} dS_{i_2 j_2} \tag{14}$$

In other words, the total interaction force between the two NURBS surfaces  $S_1$  and  $S_2$  can be obtained by summarizing interaction forces between all component NURBS patch pairs, i.e.,  $S_{i_1 j_1}$  and  $S_{i_2 j_2}$ . Hence, the initial problem is reduced to sub-problems of computing interaction forces between NURBS patch pairs. Let  $\bar{S}$  and  $\bar{\bar{S}}$  denote an arbitrary NURBS patch of surface  $S_1$  and  $S_2$ , respectively. Similar to Eq. (14), we have the interaction force between  $\bar{S}$  and  $\bar{\bar{S}}$  is

$$\bar{\mathbf{F}} = \rho_1 \rho_2 \int_{\bar{S}} \int_{\bar{\bar{S}}} (\mathbf{G} \cdot \bar{\mathbf{n}}) \cdot \bar{\bar{\mathbf{n}}} \cdot d\bar{S} d\bar{\bar{S}}.$$

From the definition of surface integral, we further have

$$\bar{\mathbf{F}} = \rho_1 \rho_2 \int_{\bar{u}_{\min}}^{\bar{u}_{\max}} \int_{\bar{v}_{\min}}^{\bar{v}_{\max}} \int_{\bar{u}_{\min}}^{\bar{u}_{\max}} \int_{\bar{v}_{\min}}^{\bar{v}_{\max}} (\mathbf{G} \cdot \bar{\mathbf{n}}) \cdot \left\| \frac{\partial \bar{S}}{\partial \bar{u}} \times \frac{\partial \bar{S}}{\partial \bar{v}} \right\| d\bar{u} d\bar{v} \cdot \bar{\mathbf{n}} \cdot \left\| \frac{\partial \bar{\bar{S}}}{\partial \bar{u}} \times \frac{\partial \bar{\bar{S}}}{\partial \bar{v}} \right\| d\bar{u} d\bar{v}, \tag{15}$$

where  $[\bar{u}_{\min} \ \bar{u}_{\max}] \times [\bar{v}_{\min} \ \bar{v}_{\max}]$  and  $[\bar{\bar{u}}_{\min} \ \bar{\bar{u}}_{\max}] \times [\bar{\bar{v}}_{\min} \ \bar{\bar{v}}_{\max}]$  represent the parametric domains of surfaces  $\bar{S}$  and  $\bar{\bar{S}}$ , respectively, the expression between vertical bars on the right-hand side is the magnitude of the cross product of the partial derivatives of  $\bar{S}$  and  $\bar{\bar{S}}$ , as shown in Fig. 3. Thus, there are only three terms in Eq. (15) that need to be further expanded, i.e.,  $\mathbf{G}$ ,  $\bar{\mathbf{n}}$  and  $\bar{\bar{\mathbf{n}}}$ . However, we know that  $\bar{\mathbf{n}}$  and  $\bar{\bar{\mathbf{n}}}$  are the unit normals of  $\bar{S}$  and  $\bar{\bar{S}}$  shown in Fig. 3. Note that, for any parametric surface  $S$  defined as a function of parameter pair  $(u, v)$ , a unit normal vector at any regular point of this surface is given as

$$\mathbf{n} = \left( \frac{\partial \mathbf{S}}{\partial u} \times \frac{\partial \mathbf{S}}{\partial v} \right) / \left\| \frac{\partial \mathbf{S}}{\partial u} \times \frac{\partial \mathbf{S}}{\partial v} \right\|. \tag{16}$$

Meanwhile, for this NURBS patch pair, the separation distance,  $s$ , from Eq. (1) can be written as:

$$s = \sqrt{(\bar{\mathbf{S}} - \bar{\bar{\mathbf{S}}}) \cdot (\bar{\mathbf{S}} - \bar{\bar{\mathbf{S}}})} \tag{17}$$

This allows us to combine Eqs. (1) and (11) to obtain the solution for the function  $\mathbf{G}$ :

$$\mathbf{G} = \frac{C \cdot (\bar{\mathbf{S}} - \bar{\bar{\mathbf{S}}})}{3 \left( (\bar{\mathbf{S}} - \bar{\bar{\mathbf{S}}}) \cdot (\bar{\mathbf{S}} - \bar{\bar{\mathbf{S}}}) \right)^{3/2}} \tag{18}$$

Hence, substituting Eqs. (16) and (18) into Eq. (15), we obtain:

$$\bar{\mathbf{F}} = \rho_1 \rho_2 \int_{\bar{u}_{\min}}^{\bar{u}_{\max}} \int_{\bar{v}_{\min}}^{\bar{v}_{\max}} \int_{\bar{u}_{\min}}^{\bar{u}_{\max}} \int_{\bar{v}_{\min}}^{\bar{v}_{\max}} \left( \frac{C \cdot (\bar{\mathbf{S}} - \bar{\bar{\mathbf{S}}})}{3 \left( (\bar{\mathbf{S}} - \bar{\bar{\mathbf{S}}}) \cdot (\bar{\mathbf{S}} - \bar{\bar{\mathbf{S}}}) \right)^{3/2}} \cdot \left( \frac{\partial \bar{S}}{\partial \bar{u}} \times \frac{\partial \bar{S}}{\partial \bar{v}} \right) \right) \cdot \left( \frac{\partial \bar{\bar{S}}}{\partial \bar{u}} \times \frac{\partial \bar{\bar{S}}}{\partial \bar{v}} \right) d\bar{u} d\bar{v} d\bar{u} d\bar{v} \tag{19}$$

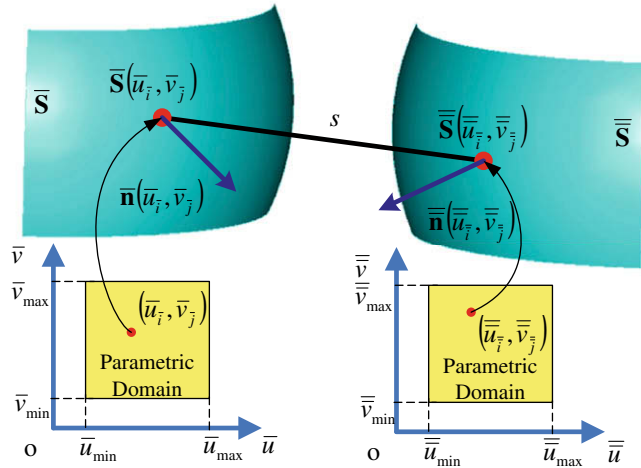


Fig. 3. Graphical illustration of a pair of NURBS patches and the terms used in calculating their interaction.

Finally, by summarizing the interaction force between each pair of NURBS patches, we can obtain the total interaction force between the two NURBS surfaces  $S_1$  and  $S_2$ .

The four-dimensional (4D) integral in Eq. (19) is still difficult for analytical evaluation. Therefore, a numerical integration method, i.e., Gaussian quadrature method, is used to approximate such a 4D integral. By implementing the Gaussian quadrature method,  $\tilde{\mathbf{F}}$  could be approximated as

$$\tilde{\mathbf{F}} = \rho_1 \rho_2 \sum_{i=1}^{\tilde{n}} \sum_{j=1}^{\tilde{m}} \sum_{\bar{i}=1}^{\bar{n}} \sum_{\bar{j}=1}^{\bar{m}} \tilde{w}(\bar{u}_i, \bar{v}_j) \cdot \tilde{w}(\bar{u}_i, \bar{v}_j) \cdot \tilde{\mathbf{f}}(\bar{u}_i, \bar{v}_j, \bar{u}_i, \bar{v}_j) \quad (20)$$

where  $\bar{n}$  and  $\bar{m}$  (respectively,  $\tilde{n}$  and  $\tilde{m}$ ) represent the number of Gaussian quadrature points in  $u$  and  $v$  direction for surface  $\bar{S}$  (respectively,  $\tilde{S}$ ),  $(\bar{u}_i, \bar{v}_j)$  and  $(\tilde{u}_i, \tilde{v}_j)$  are the Gaussian quadrature points of surfaces  $\bar{S}$  and  $\tilde{S}$ ,  $\tilde{w}$  and  $\tilde{w}$  are the corresponding weights. In this paper, we evaluate the Gaussian quadrature points and corresponding weights by the Legendre polynomials, which are defined in the interval of  $[-1, 1]$  and hence a changing of interval must be used before applying the Gaussian quadrature. And function  $\tilde{\mathbf{f}}$  is defined as

$$\tilde{\mathbf{f}}(\bar{u}, \bar{v}, \bar{u}, \bar{v}) = \left( \frac{C \cdot (\bar{\mathbf{S}}(\bar{u}, \bar{v}) - \tilde{\bar{\mathbf{S}}}(\bar{u}, \bar{v}))}{3 \left( (\bar{\mathbf{S}}(\bar{u}, \bar{v}) - \tilde{\bar{\mathbf{S}}}(\bar{u}, \bar{v})) \cdot (\bar{\mathbf{S}}(\bar{u}, \bar{v}) - \tilde{\bar{\mathbf{S}}}(\bar{u}, \bar{v})) \right)^3} \cdot \left( \frac{\partial \bar{\mathbf{S}}(\bar{u}, \bar{v})}{\partial \bar{u}} \times \frac{\partial \tilde{\bar{\mathbf{S}}}(\bar{u}, \bar{v})}{\partial \bar{v}} \right) \right) \cdot \left( \frac{\partial \tilde{\bar{\mathbf{S}}}(\bar{u}, \bar{v})}{\partial \bar{u}} \times \frac{\partial \bar{\mathbf{S}}(\bar{u}, \bar{v})}{\partial \bar{v}} \right) \quad (21)$$

where  $\bar{\mathbf{S}}(\bar{u}, \bar{v})$  and  $\tilde{\bar{\mathbf{S}}}(\bar{u}, \bar{v})$  are the expressions for NURBS surfaces, which can be evaluated by Eq. (6) with given NURBS parameters.

Similarly, for van der Waals energy between an atom/molecule and any NURBS patch  $\bar{S}$  of surface  $S_1$ , we have

$$\tilde{E} = \rho_1 \int_{\bar{u}_{\min}}^{\bar{u}_{\max}} \int_{\bar{v}_{\min}}^{\bar{v}_{\max}} \frac{C \cdot (\bar{\mathbf{S}} - \mathbf{q})}{3 \left( (\bar{\mathbf{S}} - \mathbf{q}) \cdot (\bar{\mathbf{S}} - \mathbf{q}) \right)^3} \cdot \left( \frac{\partial \bar{\mathbf{S}}}{\partial \bar{u}} \times \frac{\partial \bar{\mathbf{S}}}{\partial \bar{v}} \right) \cdot d\bar{u} d\bar{v}$$

This equation can be numerically evaluated as

$$\tilde{E} = \rho_1 \sum_{i=1}^{\bar{n}} \sum_{j=1}^{\bar{m}} \tilde{w}(\bar{u}_i, \bar{v}_j) \cdot \frac{C \cdot (\bar{\mathbf{S}}(\bar{u}_i, \bar{v}_j) - \mathbf{q})}{3 \left( (\bar{\mathbf{S}}(\bar{u}_i, \bar{v}_j) - \mathbf{q}) \cdot (\bar{\mathbf{S}}(\bar{u}_i, \bar{v}_j) - \mathbf{q}) \right)^3} \cdot \left( \frac{\partial \bar{\mathbf{S}}(\bar{u}_i, \bar{v}_j)}{\partial \bar{u}} \times \frac{\partial \bar{\mathbf{S}}(\bar{u}_i, \bar{v}_j)}{\partial \bar{v}} \right) \quad (22)$$

Such element interaction energies are then combined together as the total interaction energy between an atom/molecule and surface  $S_1$ .

## 5. Results

In this section, we validate our van der Waals force/energy calculation with four experiments where the analytical solutions are available. We then extend our approach to calculate the ellipsoid/cube interaction force, which has no reported analytical solution. Finally, we finish this section with a more complex example, which involves a flared tip in Atomic Force Microscopes (AFM) and a rough surface containing hundreds of small features. Note, in all these experiments, we adopt the physical constants from [6,7] for copper, i.e., atomic density  $\rho = 8.49 \times 10^{28} \text{ m}^{-3}$  and London–van der Waals constant  $C = 4.5639 \times 10^{-78} \text{ J m}^6$ .

### 5.1. Validation of the proposed approach

To verify the validity of the van der Waals force/energy calculation approach, we select four experiments: sphere–point van der Waals energy calculation, sphere–sphere, sphere–half space and cone–half space van der Waals force calculation, as shown in Fig. 4.

#### 5.1.1. Sphere/point

It was shown in [6,7] that the van der Waals energy between a sphere and a single molecule/atom  $q$  is determined by integrating van der Waals energy (Eq. (1)) inside the volume of the sphere with respect to the coordinates of  $q$ :

$$E_{\text{Sphere/Point}} = -\frac{\pi \cdot C \cdot \rho}{12 \cdot (d+R)} \left( \frac{2R}{(d+2R)^3} + \frac{2R}{d^3} + \frac{1}{(d+2R)^2} - \frac{1}{d^2} \right) \quad (23)$$

where  $C$  is the London–van der Waals constant,  $\rho$  is the atomic density of the sphere body,  $d$  is the closest separation between the sphere and the molecule/atom  $q$  and  $R$  is the radius of the sphere, as shown in Fig. 4a. From Eq. (23), we find that two geometric parameters, i.e., separation distance  $d$  and sphere radius  $R$ , are required for calculating the van der Waals energies for sphere–point interaction. In this experiment, the sphere radius is fixed as  $R = 100 \text{ nm}$ , twenty different separation distance  $d$  are used to cal-

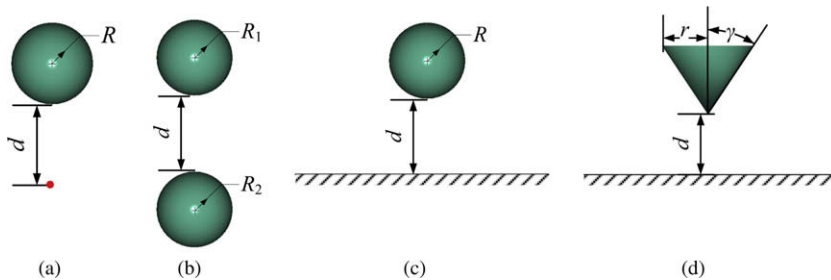
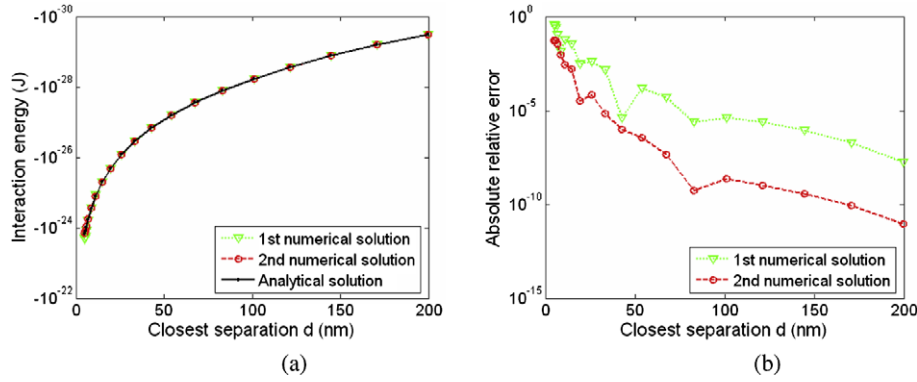


Fig. 4. Geometric configurations for four experiments. (a) Sphere–point. (b) Sphere–sphere. (c) Sphere–half space. (d) Cone–half space.



**Fig. 5.** Analytical and numerical results for sphere–point interaction energy calculation. In the first group of numerical simulation, the sphere has 32 bi-quadratic NURBS patches; In the second group, the number of surface patches is refined to 128. (a) van der Waals energy vs. separation distance. (b) Absolute relative error of our simulation results vs. separation distance.

culate the van der Waals energies, which are non-uniformly distributed from 5 nm to 200 nm.

In Fig. 5a, the analytical energy distance relation (black dot, solid line) is compared to two groups of results from the numerical integration. In the first group (green triangle, dotted line), the sphere surface consists of 32 ( $4 \times 8$ ) bi-quadratic NURBS patches (shown in Fig. 1a) and each patch is evaluated with 36 ( $6 \times 6$ ) Gaussian-Legendre quadrature points. As we can see in Fig. 5a, the values obtained by our approach follow quite well with the analytical solution. When we further examine the absolute relative errors (i.e., the difference between the nominal value and the calculated value divided by the nominal value) in Fig. 5b, we observe a downward trend as the separation distance increases. We also find a relative large error (>5%) as the separation distance  $d$  falls under 10 nm. This suggests closer separation may require finer patches.

Therefore, in order to improve the simulation accuracy, in the second group (red circle, dashed line), we refine the sphere surface into 128 ( $8 \times 16$ ) NURBS patches and the number of quadrature points per patch remains the same. In Fig. 5b, we can see that by increasing the number of NURBS patches, an average of one order of magnitude better accuracy is achieved in comparison with the first group. However, increasing patch number also results in increased computational complexity and thus the time (four times as the first group).

### 5.1.2. Sphere/sphere

In a system of two nano spherical particles 1 and 2 of radii  $R_1$  and  $R_2$  (shown in Fig. 4b), with a separation of  $d$ , the non-retarded van der Waals force between two spheres is [5]:

$$F_{\text{Sphere/Sphere}} = -\frac{A \cdot (d + R_1 + R_2)}{3} \left( -\frac{1}{2d \cdot (R_1 + R_2)} + \frac{1}{4R_1R_2} + \frac{1}{4d^2 \cdot (R_1 + R_2)^2} + \frac{R_1R_2}{8R_1R_2} \right) \quad (24)$$

From Eq. (24), we find that three geometric parameters, i.e., separation distance  $d$  and sphere radii  $R_1$  and  $R_2$ , are required to calculate the van der Waals forces for sphere–sphere interaction. In this experiment, we adopt the same separation distance  $d$  as the previous experiment and fix the sphere radii as  $R_1 = R_2 = 100$  nm.

Similar to the previous experiment, the analytical solution (black dot, solid line) is compared to two groups of numerical results: in the first group (green triangle, dotted line), the two sphere surfaces are composed of 32 ( $4 \times 8$ ) bi-quadratic NURBS patches (shown in Fig. 1a) and each patch is evaluated with 36 ( $6 \times 6$ ) quadrature points; in the second group (red circle, dashed line), the number of NURBS patches in each sphere is increased to 128 ( $8 \times 16$ ), as shown in Fig. 1b. The experimental results in Fig. 6 demonstrate that (a) the NURBS surface based approach yields accurate results, and (b) patch refinements improves the calculation accuracy.

### 5.1.3. Sphere/half space

It was given in [6,7] that the non-retarded van der Waals force between a sphere and a half space is

$$F_{\text{Sphere/Plane}} = -\frac{2A \cdot R^3}{3d^2 \cdot (d + 2R)^2} \quad (25)$$

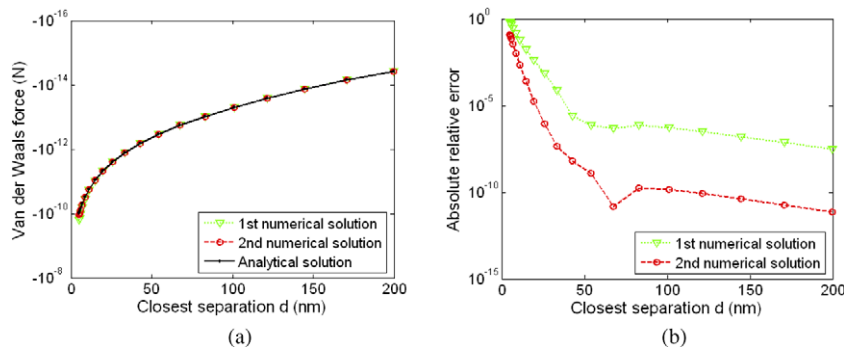


**Fig. 6.** Analytical and numerical results for sphere–sphere interaction force calculation. In the first group of numerical results, each of the two spheres has 32 bi-quadratic NURBS patches. In the second group, the number of surface patches is refined to 128. (a) van der Waals force vs. separation distance. (b) Absolute relative error of our simulation results vs. separation distance.

where  $d$  is the closest separation between the sphere and the half space and  $R$  is the radius of the sphere, shown in Fig. 4(c).

In the experiment for sphere–half space interaction force calculation, the sphere, with a radius of  $R = 100$  nm, is composed of 32 ( $4 \times 8$ ) bi-quadratic NURBS patches (shown in Fig. 1a) and each patch is evaluated with 36 ( $6 \times 6$ ) quadrature points. To represent the boundary plane of a half space, a plane with a dimension of  $400 \text{ nm} \times 400 \text{ nm}$ , i.e., far from being infinite, is adopted, which consists of 36 ( $6 \times 6$ ) bi-linear NURBS patches and each patch is evaluated with 36 ( $6 \times 6$ ) quadrature points. The results are shown in Fig. 7.

From Fig. 7b, we can observe that the error decreases initially with the increased separation distance. However, after a turning point, the error increases with the separation distance (green triangle, dotted line), when the separation is around 25 nm. We believe that this turning point is due to the dimension of the plane. When the separation  $d$  is comparable to the plane edge length, the chosen plane cannot approximate an infinite plane well and hence produce a large error.

To verify this, we enlarge the plane to a dimension of  $800 \text{ nm} \times 800 \text{ nm}$ . Meanwhile, we have to increase the number of patches to 144, in order to maintain the size of each surface patch. Using this enlarged plane, we generate the second group of results (red circle, dashed line). In Fig. 7b, we can find that the original large errors at the separations larger than 50 nm are reduced significantly and an average of two order of magnitude better accuracy is achieved.

#### 5.1.4. Cone/half space

In [2], Argento and French constructed a parametric tip model with a cone-shape and derived the interaction force between a cone and a half space as

$$F_{\text{Cone/Plane}} = -\frac{A \cdot r^2 \cdot \sin(\gamma)}{6d \cdot \cos(\gamma) \cdot \cot(\gamma) \cdot (r + d \cdot \tan(\gamma))^2} \quad (26)$$

where  $d$  is the closest separation between the cone and the half space,  $r$  is the radius of cone base and  $\gamma$  is the cone angle, as shown in Fig. 4(d).

In the experiment for cone–half space interaction force calculation and comparison, we adopt the same original and enlarged planes as in the previous experiment. The cone surface has a base radius of  $r = 150$  nm and a cone angle of  $\gamma = 45^\circ$ . This NURBS surface, which is linear in  $u$  direction and quadratic in  $v$  direction, is composed of 64 ( $4 \times 16$ ) NURBS patches and each patch is evaluated with 36 ( $6 \times 6$ ) quadrature points.

The results shown in Fig. 8 demonstrate that the NURBS surface based approach produces results consistent with the analytical

solution. When the separation distance becomes larger, the corresponding plane size for the half space should be enlarged accordingly to ensure the accuracy.

#### 5.2. Example for simple geometries with no known analytical solution

Close form formulas of van der Waals energies/forces are still not yet possible for many simple object geometries. In this subsection, we calculate the interaction force between an ellipsoid and a cube, which has no reported analytical solution.

In Fig. 9a, an ellipsoid is defined by two geometry parameters, i.e., major radius  $R_{ma} = 100$  nm and minor radius  $R_{mi} = 100$  nm; a cube is defined by the edge length, i.e.,  $l = 400$  nm. In this example, the ellipsoid is composed of 128 ( $8 \times 16$ ) bi-quadratic NURBS patches and the cube is composed of 216 ( $6 \times 6 \times 6$ ) bi-linear NURBS patches. These two objects are placed at 20 different separation distance  $d$ , which are identical to the separation in the previous experiments. Note that the center of the cube is located on the major axis of the ellipsoid and one pair of the cube faces are perpendicular to this axis, as shown in Fig. 9a. The results are plotted in Fig. 9b, where the  $x$  axis represents the separation distance and  $y$  axis represents the van der Waals force.

#### 5.3. Example for complex geometries

We finish this section with an example on complex geometries. In this example, we calculate the interaction energy between a rough surface and a flared tip (Fig. 10). The flared tip is composed of 34 bi-cubic NURBS patches. The rough surface consists of 900 ( $30 \times 30$ ) bi-quadratic NURBS patches. The resulting interaction force is  $3.2107 \times 10^{-14}$  N and the energy distribution is shown in Fig. 10b as a color map.

## 6. Discussion

In this section, we compare our NURBS surface based numerical integration approach with triangle mesh based approach. We also examine further the influence of patch size over calculation accuracy and its implication.

#### 6.1. Comparison with triangular mesh based numerical integration

The London equation (Eq. (1)) shows an inverse sixth-power law relationship between distance  $s$  and energy potential of two atoms/molecules. Thus the energy potential is very sensitive to the distance. A small deviation in distance may result in a large error in the resulting energy/force calculation. To illustrate this, we

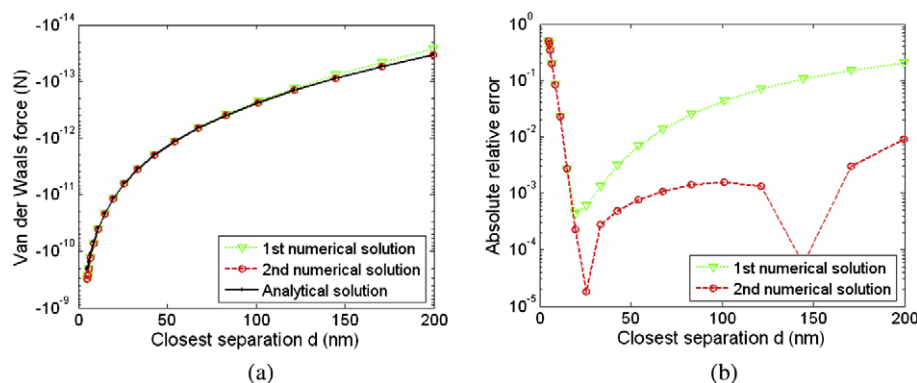


**Fig. 7.** Analytical and numerical results for sphere–half space interaction force calculation. In the first group, the plane has a dimension of  $400 \text{ nm} \times 400 \text{ nm}$ . In the second group, its dimension is extended to  $800 \text{ nm} \times 800 \text{ nm}$ . (a) van der Waals force vs. separation distance. (b) Absolute relative error of our simulation results vs. separation distance.

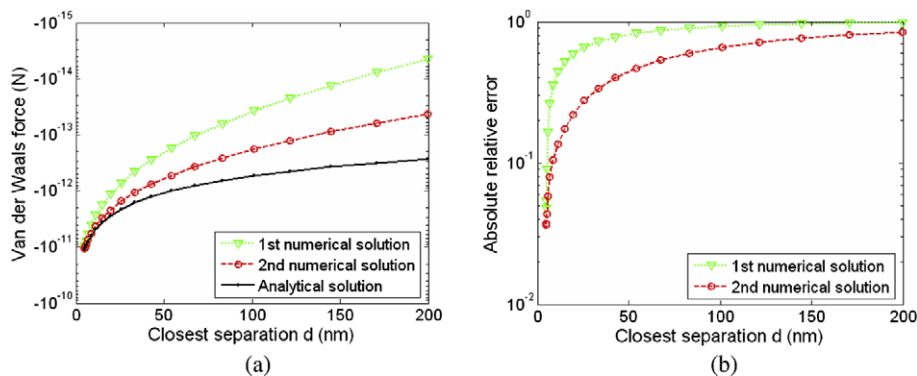


**Fig. 8.** Analytical and numerical results for cone–half space interaction force calculation. In the first group, the plane has a dimension of  $400 \text{ nm} \times 400 \text{ nm}$ . In the second group, its dimension is extended to  $800 \text{ nm} \times 800 \text{ nm}$ . (a) van der Waals force vs. separation distance. (b) Absolute relative error of our simulation results vs. separation distance.

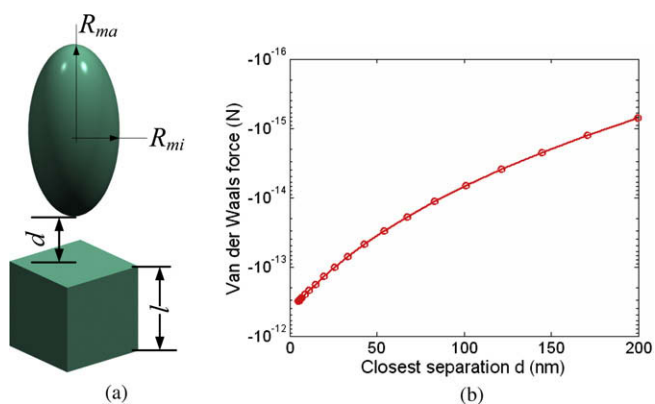


**Fig. 9.** Example of ellipsoid–cube interaction force calculation. (a) Geometry configuration. (b) van der Waals force vs. separation distance.

compare our NURBS surface based approach where the geometry is represented exactly with triangulate mesh based approach where curved object geometry is approximated with planar triangles.

The comparison is based on the sphere–sphere van der Waals force calculation. In the NURBS based approach, we adopt all the parameters of the first group of numerical results in Section 5.1.2, that is, the sphere (shown in Fig. 11a) is composed of 128 ( $8 \times 16$ ) bi-quadratic NURBS patches and each patch is evaluated with 36 ( $6 \times 6$ ) quadrature points. To set up a fair comparison, the triangle mesh (shown in Fig. 11b) was generated by dividing each of the NURBS patches in the first group into two triangles, where the triangle vertexes are given by the patch vertexes and the two triangles share two diagonal points of the patch. Meanwhile, we set the number of quadrature points for each triangle

as  $6 \times 3$ , which would keep the total number of quadrature points the same as in the NURBS based approach, i.e., same amount of computation.

The results show that the NURBS based approach is much more accurate than the triangular mesh based approach. Fig. 11(c) illustrates a gap between the triangular mesh based results (green triangle, dotted line) and the analytical solutions (black dot, solid line) but the results of the NURBS based approach (red circle, dashed line) fit the analytical solutions very well. Fig. 11d shows an order of magnitude better accuracy is achieved with the NURBS based approach over the triangle mesh based approach.

### 6.2. Efficiency improvement with adaptive surface subdivision

In Section 5, we showed that, by refining (subdividing) NURBS surfaces, the force calculation accuracy is improved. However, the increase of the NURBS surface patches increases the computation time. In this section, we discuss how to improve the calculation accuracy without increasing the number of patches. The basic insight is that not all the surface patches have the same contribution to the calculation result. By using finer surface patches (via more subdivisions) at regions with high contributions and using coarse surface patches (i.e., fewer subdivisions) at regions with the low contributions, we can achieve both high accuracy and high efficiency in van der Waals force/energy calculation. More specifically, the distance  $s$  can be used as a criterion to determine patch subdivision since the distance  $s$  and the energy potential of two atoms/molecules have an inverse sixth-power law relationship.

To illustrate this, we adopt the sphere and atom/molecule interact energy calculation as an example. As shown in Fig. 12, two cases of van der Waals energy calculation are shown here, where the two spherical surfaces are identical but the relative position

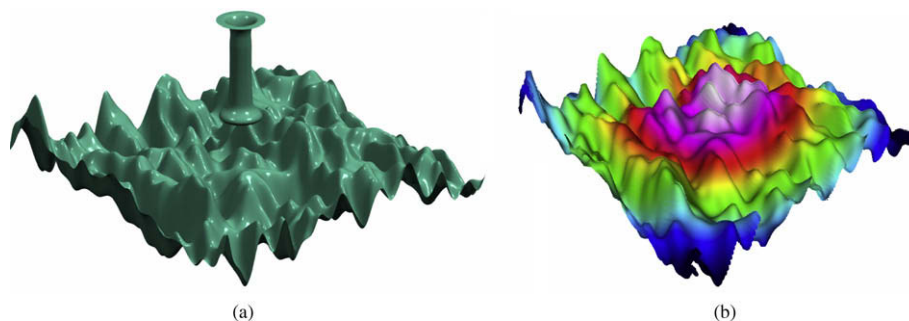


**Fig. 10.** Interaction energy between a flared AFM tip and rough surface. (a) Geometry configuration. (b) Distribution of van der Waals energies.

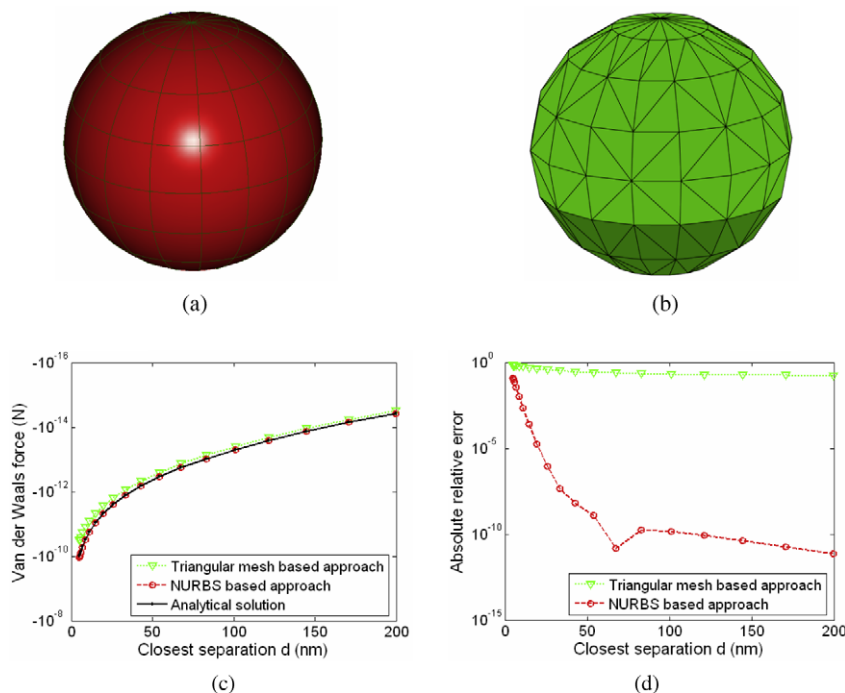


**Fig. 11.** Comparing triangular mesh based approach and NURBS surface based approach on sphere–sphere van der Waals force calculation. (a) An NURBS surface represents the sphere exactly. (b) A triangular mesh approximates the sphere. (c) van der Waals force vs. separation distance. (d) Absolute relative error of our simulation results vs. separation distance.

between the spheres and the atom/molecule are different: in Case one (green triangle, dotted line), the atom/molecule point faced the coarse region; in Case two (red circle, dashed line), the atom/molecule point faced the fine region. The comparison results are shown in Fig. 12b and c, where we can find an average four orders of magnitude better accuracy is achieved with Case two ( $9.8447\text{e-}6$ ) over Case one (0.1077). This suggests that a proper adaptive surface subdivision scheme can dramatically improve the efficiency of the van der Waals force/energy calculation without compromising the accuracy.

### 6.3. Error estimation and convergence analysis

The results in Section 5 show the NURBS based approach can provide accurate calculation. We here discuss the error estimation in the numerical procedure. In the section, we introduce two kinds of error estimation approaches, i.e., a priori approach and a posteriori approach:

- *A priori approach.* From Eq. (19), we find a positive relationship between the magnitude of the interaction force  $|\bar{F}_{12}|$  and the areas  $M_1, M_2$  of surface  $S_1, S_2$ . We also find a negative relationship between  $|\bar{F}_{12}|$  and the geometric distance  $D$  of two points on the two surface  $S_1, S_2$ . However, the surface area  $M_1$  and  $M_2$  could be accurately determined with an error bound; and the minimum value of the geometric distance  $D$  can be obtained based on the NURBS Property 2. Hence, we can determine an upper bound of  $|\bar{F}_{12}|$  with the upper bound of  $M_1, M_2$  and the lower bound of  $D$ . It can be used to calculate the estimated error.
- *A posteriori approach.* Suppose we have a pair of initial NURBS surface  $S_1$  and  $S_2$ . Then based on the interaction force calculation scheme introduced in this paper, we can calculate an initial interaction force  $\mathbf{F}_{12}$ . To estimate the accuracy of this force, we first generate a more precise numerical model, which can be achieved via two steps: (1) generating a new surface pair  $\bar{S}_1, \bar{S}_2$  by refining the initial surface  $S_1, S_2$ , i.e., subdividing each surface

patch into four sub-patches; (2) increasing the number of Gaussian quadrature points, e.g., from  $n \times n$  to  $2n \times 2n$ . For this refined model, we can calculate a new interaction force  $\bar{\mathbf{F}}_{12}$ . Then the estimated computational error can be defined as

$$e_{12} = \frac{\|\bar{\mathbf{F}}_{12}\| - \|\mathbf{F}_{12}\|}{\|\bar{\mathbf{F}}_{12}\|}$$

In this paper, we adopt the second approach for error estimation and convergence analysis. A brief error estimation and convergence analysis is given in Table 2 for the plane/cone interaction. It shows the convergence of this process. Note, a detailed description of the calculation of the plane/cone interaction and the source code is in Appendix A.

## 7. Conclusions

In this paper, we have developed a NURBS surface based approach for calculating van der Waals force and energy between macroscopic objects. The calculation is based on the surface formulation where the original 6D volume integration is converted into 4D surface integration. The integration is done through the Gauss-

**Table 2**  
Error estimation and convergence analysis for the plane/cone interaction force calculation.

Number of patches		Number of quadrature points for each patch	Interaction force (N)	Error estimation with the posteriori approach (%)
Plane	Cone			
1 (1 × 1)	4 (4 × 1)	2 × 2	$1.0212 \times 10^{-13}$	24.86
1 (1 × 1)	4 (4 × 1)	4 × 4	$1.3591 \times 10^{-13}$	2.08
4 (2 × 2)	16 (8 × 2)	4 × 4	$1.3879 \times 10^{-13}$	0.0072
4 (2 × 2)	16 (8 × 2)	8 × 8	$1.3880 \times 10^{-13}$	–

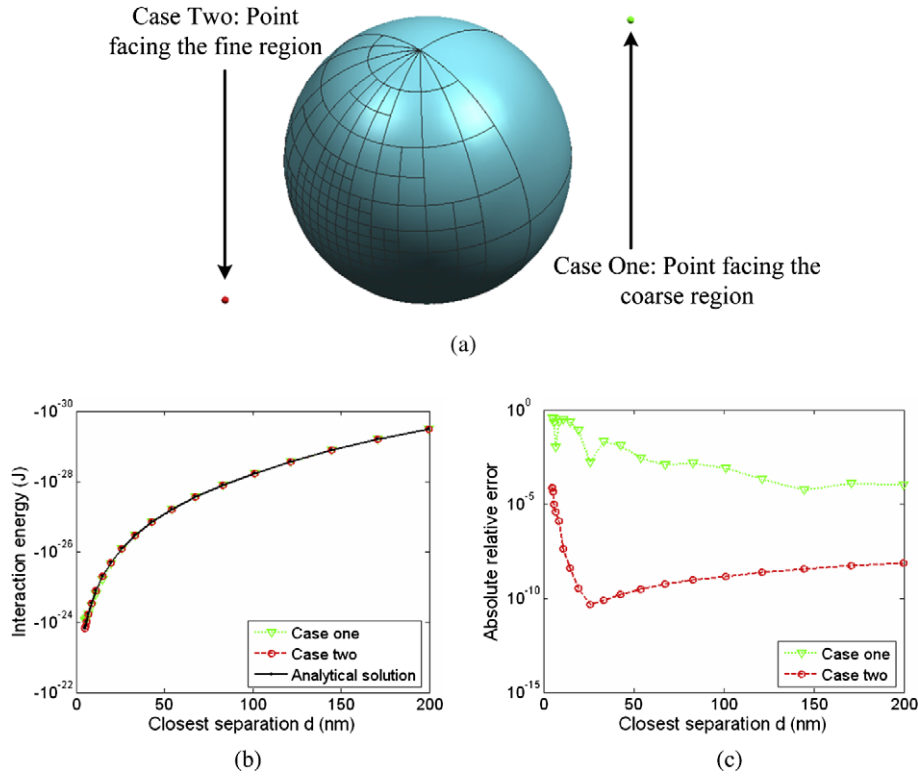


**Fig. 12.** Comparison of sphere–point interaction energies in two different cases: point facing the coarse region (Case one) and point facing the fine region (Case two). (a) Relative position and orientation of the sphere and the atom/molecule in these two cases. (b) van der Waals energy vs. separation distance. (c) Absolute relative error of our simulation results vs. separation distance.

ian quadrature method where the Gaussian quadrature points lie exactly on the object surface. The key advantages of this approach include its applicability to various geometries and high calculation efficiency.

We implemented the NURBS surface based approach and compared the results on common geometries where analytical solutions exist. The comparison validates that the NURBS surface based approach produces accurate results.

**Appendix A. Tutorial on NURBS based van Der Waals force calculation**

In this appendix, we use the calculation of Cone/Half space interaction force as an example to explain our approach in detail. This approach is implemented with Matlab and the source code is available at <http://www.mmae.iit.edu/cadcam/code/>.

In this tutorial example, we will adopt the same geometric configuration as given in Section 5.1.4, i.e., the cone base radius  $r = 200$  nm, the cone angle  $\gamma = 45^\circ$  and the length of the plane  $l = 400$  nm. However, to make a simpler example, we will fix the closest separation  $d$  to 100 nm and adopt NURBS representations for the plane and the cone, as illustrated in Table 3. Meanwhile, a  $2 \times 2$  quadrature points will be used to evaluate the patch to patch interaction force.

From Table 3, we find that the plane surface contains no inner knots, which means that it is composed with a single NURBS patch  $\mathbf{S}_{plane}(\bar{u}, \bar{v})$ , as shown in Fig. 13. Meanwhile, we find that the cone surface contains three unique inner knots in  $u$  direction, i.e., 0.25, 0.5, 0.75, which, according to NURBS surface Property 3, divide the cone surface into four parts. From the definition of basis functions in Eqs. (7)–(10), we find that for each of these four patches, there are only six basis functions are non-zero functions. For example, for the first patch defined on  $[01/4] \times [01]$  (the yellow surface

**Table 3**  
NURBS surface parameters for the plane and the cone.

Surface type	Degree		Knot vector		Control points, $\mathbf{p}_{i,j}$	Weights $w_{i,j}$
	$u$	$v$	$u$	$v$		
Plane	1	1	{0, 0, 1, 1}	{0, 0, 1, 1}	$\mathbf{p}_{0,0} = (-200, -200, -100)$ , $\mathbf{p}_{1,0} = (200, -200, -100)$ , $\mathbf{p}_{0,1} = (-200, 200, -100)$ , $\mathbf{p}_{1,1} = (200, 200, -100)$	$w_{i,j} = 1$
Cone	2	1	{0, 0, 0, 0.25, 0.25, 0.5, 0.5, 0.75, 0.75, 1, 1, 1}	{0, 0, 1, 1}	$\mathbf{p}_{i,0} = (0, 0, 0)$ , $i = 0, 1, 2, 3, 4, 5, 6, 7, 8$ .  $\mathbf{p}_{0,1} = \mathbf{p}_{8,1} = (150, 0, 150)$ , $\mathbf{p}_{1,1} = (150, 150, 150)$ , $\mathbf{p}_{2,1} = (0, 150, 150)$ , $\mathbf{p}_{3,1} = (-150, 150, 150)$ , $\mathbf{p}_{4,1} = (-150, 0, 150)$ , $\mathbf{p}_{5,1} = (-150, -150, 150)$ , $\mathbf{p}_{6,1} = (0, -150, 150)$ , $\mathbf{p}_{7,1} = (150, -150, 150)$ .	$w_{i,j} = 1, i = 0, 2, 4, 6, 8, j = 0, 1$ .  $w_{i,j} = \frac{\sqrt{2}}{2}, i = 1, 3, 5, 7, j = 0, 1$ .

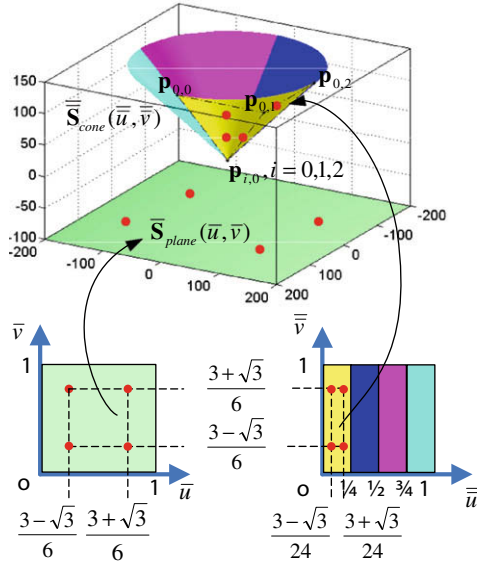


Fig. 13. Graphical illustration of the plane, the cone and the terms used in calculating their interaction.

patch shown in Fig. 13), the six non-zero basis functions are  $N_{i,0}, N_{0,j}, i, j = 0, 1, 2$ , which means that the patch is determined by these six basis functions and corresponding control points. In this example, without loss of generality, we will go through the calculation of the interaction force between the first patch  $\bar{\mathbf{S}}_{\text{cone}}(\bar{u}, \bar{v})$  and  $\bar{\mathbf{S}}_{\text{plane}}(\bar{u}, \bar{v})$  in details. Note, the interaction forces between the other patches and  $\bar{\mathbf{S}}_{\text{plane}}(\bar{u}, \bar{v})$  can be calculated with a similar procedure. The sum of these four forces gives the total interaction force between the plane and cone.

In this example, a  $2 \times 2$  quadrature points is used to evaluate the patch to patch interaction force. For a standard 2-nodes Gaussian-Legendre quadrature for an integral over  $[-1, 1]$ , we have the quadrature nodes are  $\pm \frac{\sqrt{3}}{2}$  and the corresponding weights are  $1/2$ . However, in this example, surface  $\bar{\mathbf{S}}_{\text{plane}}(\bar{u}, \bar{v})$  is defined on the parametrical domain  $[0, 1] \times [0, 1]$  and surface  $\bar{\mathbf{S}}_{\text{cone}}(\bar{u}, \bar{v})$  is defined on  $[0, 1/4] \times [0, 1]$ . Hence, a change of interval for Gaussian quadrature must be applied. Suppose an integral over  $[a, b]$  must be changed into an integral over  $[-1, 1]$ , the change of interval can be done in the following way:

$$\begin{cases} x' = \frac{(b-a)x + a+b}{2} \\ y' = \frac{b-a}{2}y \end{cases} \quad (27)$$

where  $x$  and  $x'$  (respectively,  $y$  and  $y'$ ) are the quadrature nodes (respectively, weights) in the original domain  $[-1, 1]$  and the new domain  $[a, b]$ . Substituting these into Eq. (20), the interaction force between  $\bar{\mathbf{S}}_{\text{plane}}(\bar{u}, \bar{v})$  and  $\bar{\mathbf{S}}_{\text{cone}}(\bar{u}, \bar{v})$  can be numerically evaluated as

$$\begin{aligned} \tilde{\mathbf{F}} &= \rho^2 \cdot \frac{1}{64} \cdot \sum_{i=1}^2 \sum_{j=1}^2 \sum_{i=1}^2 \sum_{j=1}^2 \bar{w} \left( \frac{\bar{u}'_i + 1}{2}, \frac{\bar{v}'_j + 1}{2} \right) \\ &\quad \cdot \bar{w} \left( \frac{\bar{u}'_i + 1}{8}, \frac{\bar{v}'_j + 1}{2} \right) \cdot \bar{\mathbf{f}} \left( \frac{\bar{u}'_i + 1}{2}, \frac{\bar{v}'_j + 1}{2}, \frac{\bar{u}'_i + 1}{8}, \frac{\bar{v}'_j + 1}{2} \right) \\ &= \frac{\rho^2}{1024} \cdot \sum_{i=1}^2 \sum_{j=1}^2 \sum_{i=1}^2 \sum_{j=1}^2 \bar{\mathbf{f}} \left( \frac{\bar{u}'_i + 1}{2}, \frac{\bar{v}'_j + 1}{2}, \frac{\bar{u}'_i + 1}{8}, \frac{\bar{v}'_j + 1}{2} \right) \end{aligned} \quad (28)$$

where  $\bar{u}'_1 = \bar{v}'_1 = \bar{u}'_1 = \bar{v}'_1 = \frac{\sqrt{3}}{3}$  and  $\bar{u}'_2 = \bar{v}'_2 = \bar{u}'_2 = \bar{v}'_2 = -\frac{\sqrt{3}}{3}$  are the original nodes.

To evaluate function  $\bar{\mathbf{f}}$  with Eq. (21), we still need to know the expressions of  $\bar{\mathbf{S}}_{\text{plane}}(\bar{u}, \bar{v})$ ,  $\bar{\mathbf{S}}_{\text{cone}}(\bar{u}, \bar{v})$  and their first partial deriva-

tives, which can be calculated with a fast and numerically stable algorithm, i.e., Cox-DeBoor algorithm. Meanwhile, they can also be evaluated based on the definition of NURBS surface. In this example, by substituting the parameters of the plane surface into Eqs. (6)–(10), we apply the latter method and get the parametric representation of  $\bar{\mathbf{S}}_{\text{plane}}(\bar{u}, \bar{v})$  as:

$$\begin{aligned} \bar{\mathbf{S}}_{\text{plane}}(\bar{u}, \bar{v}) &= (1 - \bar{u})(1 - \bar{v}) \cdot \mathbf{p}_{0,0} + \bar{u}(1 - \bar{v}) \cdot \mathbf{p}_{1,0} + (1 - \bar{u})\bar{v} \cdot \mathbf{p}_{0,1} \\ &\quad + \bar{u}\bar{v} \cdot \mathbf{p}_{1,1} = \begin{pmatrix} 200(2 \cdot \bar{u} - 1) \\ 200(2 \cdot \bar{v} - 1) \\ -100 \end{pmatrix}, \bar{u}, \bar{v} \in [0, 1]. \end{aligned} \quad (29)$$

Similarly, we have

$$\begin{aligned} \bar{\mathbf{S}}_{\text{cone}}(\bar{u}, \bar{v}) &= \frac{(1 - \bar{v}) \cdot ((1 - 4 \cdot \bar{u})^2 \cdot \mathbf{p}_{0,0} + 4\sqrt{2} \cdot \bar{u}(1 - \bar{u}) \cdot \mathbf{p}_{1,0} + 16 \cdot \bar{u}^2 \cdot \mathbf{p}_{2,0})}{(1 - 4 \cdot \bar{u})^2 + 4\sqrt{2} \cdot \bar{u}(1 - \bar{u}) + 16 \cdot \bar{u}^2} \\ &\quad + \frac{\bar{v} \cdot ((1 - 4 \cdot \bar{u})^2 \cdot \mathbf{p}_{0,1} + 4\sqrt{2} \cdot \bar{u}(1 - \bar{u}) \cdot \mathbf{p}_{1,1} + 16 \cdot \bar{u}^2 \cdot \mathbf{p}_{2,1})}{(1 - 4 \cdot \bar{u})^2 + 4\sqrt{2} \cdot \bar{u}(1 - \bar{u}) + 16 \cdot \bar{u}^2} \\ &= \frac{\bar{v} \cdot \begin{pmatrix} 150 \cdot (1 - 4 \cdot \bar{u})^2 + 600\sqrt{2} \cdot \bar{u}(1 - \bar{u}) \\ 600\sqrt{2} \cdot \bar{u}(1 - \bar{u}) + 2400 \cdot \bar{u}^2 \\ 150 \cdot (1 - 4 \cdot \bar{u})^2 + 600\sqrt{2} \cdot \bar{u}(1 - \bar{u}) + 2400 \cdot \bar{u}^2 \end{pmatrix}}{(1 - 4 \cdot \bar{u})^2 + 4\sqrt{2} \cdot \bar{u}(1 - \bar{u}) + 16 \cdot \bar{u}^2}, \\ &\quad \bar{u} \in [0, \frac{1}{4}], \bar{v} \in [0, 1]. \end{aligned} \quad (30)$$

Taking partial derivatives of Eq. (29) with respect to  $\bar{u}$  and  $\bar{v}$ , we get

$$\frac{\partial \bar{\mathbf{S}}_{\text{plane}}(\bar{u}, \bar{v})}{\partial \bar{u}} = \begin{pmatrix} 400 \\ 0 \\ 0 \end{pmatrix}, \quad \frac{\partial \bar{\mathbf{S}}_{\text{plane}}(\bar{u}, \bar{v})}{\partial \bar{v}} = \begin{pmatrix} 0 \\ 400 \\ 0 \end{pmatrix} \quad (31)$$

Taking partial derivatives of Eq. (30) with respect to  $\bar{u}$  and  $\bar{v}$ , we get

$$\begin{aligned} \frac{\partial \bar{\mathbf{S}}_{\text{cone}}(\bar{u}, \bar{v})}{\partial \bar{u}} &= \frac{v \cdot \begin{pmatrix} -4800 \cdot u \cdot ((2\sqrt{2} - 4) \cdot \bar{u} + 1) \\ 600 \cdot ((16\sqrt{2} - 32) \cdot \bar{u}^2 + (8 - 8\sqrt{2}) \cdot \bar{u} + \sqrt{2}) \end{pmatrix}}{((16\sqrt{2} - 32) \cdot \bar{u}^2 + (8 - 4\sqrt{2}) \cdot \bar{u} - 1)^2} \\ \frac{\partial \bar{\mathbf{S}}_{\text{cone}}(\bar{u}, \bar{v})}{\partial \bar{v}} &= \frac{\begin{pmatrix} 150 \cdot (1 - 4 \cdot \bar{u})^2 + 600\sqrt{2} \cdot \bar{u}(1 - \bar{u}) \\ 600\sqrt{2} \cdot \bar{u}(1 - \bar{u}) + 2400 \cdot \bar{u}^2 \\ 150 \cdot (1 - 4 \cdot \bar{u})^2 + 600\sqrt{2} \cdot \bar{u}(1 - \bar{u}) + 2400 \cdot \bar{u}^2 \end{pmatrix}}{(1 - 4 \cdot \bar{u})^2 + 4\sqrt{2} \cdot \bar{u}(1 - \bar{u}) + 16 \cdot \bar{u}^2} \end{aligned} \quad (32)$$

Once we got these expressions, we are ready to calculate the “point to point” van der Waals force, i.e.,  $\bar{\mathbf{f}}$ , with Eq. (21). Since in this example, both surfaces are evaluated with  $2 \times 2$  quadrature points, we need to calculate the interaction force  $\bar{\mathbf{f}}$  for all the point to point pairs, that is sixteen times of evaluation, whose sum gives the total interaction force between  $\bar{\mathbf{S}}_{\text{plane}}(\bar{u}, \bar{v})$  and  $\bar{\mathbf{S}}_{\text{cone}}(\bar{u}, \bar{v})$  as  $F_1 = 2.5529 \times 10^{-14}$  N. Applying a similar procedure to calculate the interaction forces between the other three patches of the cone surface and  $\bar{\mathbf{S}}_{\text{plane}}(\bar{u}, \bar{v})$  and adding them together, we get the total interaction force between the plane and the cone is  $F_{pc} = 1.0212 \times 10^{-13}$  N, whose accuracy can be further improved by increasing the number of surface patches or the number of quadrature points.

## References

- [1] A. Anandarajah, J. Chen, *Journal of Colloid Interface Science* 176 (2) (1995) 293.
- [2] C. Argento, R.H. French, *Journal of Applied Physics* 80 (1996) 6081.
- [3] C. Argento, A. Jagota, W.C. Carter, *Journal of the Mechanics and Physics of Solids* 45 (7) (1997) 1161.
- [4] S. Bhattacharjee, M.J. Elimelech, *Journal of Colloid Interface Science* 193 (2) (1997) 273.
- [5] J. Chen, A. Anandarajah, *Journal of Colloid Interface Science* 180 (1996) 519.
- [6] J.T. Feddema, *Journal of Micromechatronics* (2001) 139.
- [7] J.T. Feddema, P. Xavier, R. Brown, Assembly planning at the micro scale, in: *Proceedings of the Workshop on Precision Manipulation at the Micro and Nano Scales, 1998 IEEE International Conference on Robotics and Automation, Leuven, Belgium*, pp. 56–69, 1998.
- [8] J.N. Israelachvili, *Contemporary Physics* 15 (2) (1974) 159.
- [9] A. Menciassi, A. Eisinger, I. Izzo, P. Dario, *IEEE/ASME Transactions on Mechatronics* 9 (2) (2004) 311.
- [10] S.W. Montgomery, M.A. Franczek, V.W. Goldschmidt, *Journal of Colloid Interface Science* 227 (2) (2000) 567–584. July.
- [11] L. Piegl, W. Tiller, *The NURBS Book*, second ed., Springer-Verlag, New York, 1997.
- [12] M.B. Ranade, *Aerosol Science and Technology* 7 (1987) 161.
- [13] M. Savia, Z. Quan, Simulating adhesion forces between arbitrarily shaped objects in micro/nano-handling operations, in: *Proceedings of the 2004 IEEE/RSJ International Conference on Intelligent Robots and Systems*, pp. 1722–1727, 2004.
- [14] L. Suresh, J.Y. Walz, *Journal of Colloid Interface Science* 183 (1) (1996) 199. October.